Title

Antagonism between the dynein and Ndc80 complexes at kinetochores controls the stability of kinetochore–microtubule attachments during mitosis

Journal

Journal of Biological Chemistry, 293(16)

ISSN

0021-9258

Authors

Amin, Mohammed A
McKenney, Richard J
Varma, Dileep

Publication Date

2018-04-01

DOI

10.1074/jbc.ra117.001699

Peer reviewed

Antagonism between the dynein and Ndc80 complexes at kinetochores controls the stability of kinetochore–microtubule attachments during mitosis

Received for publication, December 29, 2017, and in revised form, February 6, 2018 Published, Papers in Press, February 23, 2018, DOI 10.1074/jbc.RA117.001699

Mohammed A. Amin[‡], **Richard J. McKenney**[§], **and Dileep Varma**[‡1]

From the [‡]*Department of Cell and Molecular Biology, Feinberg School of Medicine, Northwestern University, Chicago, Illinois 60611 and* [§]*Department of Molecular and Cellular Biology, University of California, Davis, California 95616*

Edited by Phyllis I. Hanson

Chromosome alignment and segregation during mitosis require kinetochore–microtubule (kMT) attachments that are mediated by the molecular motor dynein and the kMT-binding complex Ndc80. The Rod–ZW10–Zwilch (RZZ) complex is central to this coordination as it has an important role in dynein recruitment and has recently been reported to have a key function in the regulation of stable kMT attachments in *Caenorhabditis elegans* besides its role in activating the spindle assembly checkpoint (SAC). However, the mechanism by which these protein complexes control kMT attachments to drive chromosome motility during early mitosis is still unclear. Here, using *in vitro* total internal reflection fluorescence microscopy, we observed that higher concentrations of Ndc80 inhibited dynein binding to MTs, providing evidence that Ndc80 and dynein antagonize each other's function. High-resolution microscopy and siRNA-mediated functional disruption revealed that severe defects in chromosome alignment induced by depletion of dynein or the dynein adapter Spindly are rescued by codepletion of the RZZ component Rod in human cells. Interestingly, rescue of the chromosome alignment defects was independent of Rod function in SAC activation and was accompanied by a remarkable restoration of stable kMT attachments. Furthermore, the chromosome alignment rescue depended on the plus-end–directed motility of centromere protein E (CENP-E) because cells codepleted of CENP-E, Rod, and dynein could not establish stable kMT attachments or align their chromosomes properly. Our findings support the idea that dynein may control the function of the Ndc80 complex in stabilizing kMT attachments directly by interfering with Ndc80–MT binding or indirectly by controlling the Rod-mediated inhibition of Ndc80.

Faithful chromosome segregation during mitosis requires proper chromosome congression, which relies on multiple mechanisms that ultimately lead to chromosome biorientation, an arrangement where the chromosomes are connected to microtubules from both spindle poles (1). In the classical "search and capture" model, chromosomes move toward the spindle equator as a result of their biorientation (2). After nuclear envelope breakdown (NEB),[2] chromosomes are known to congress by two main mechanisms: microtubule polymerization/depolymerization–based motion (3) and motor-dependent transport along microtubules achieved by the coordinated activities of dynein, CENP-E, and chromokinesins (4–6). The peripheral chromosomes are first transported by dynein to a microtubule-dense region near the spindle pole from where they move toward the spindle equator along pre-existing spindle microtubules with the help of the CENP-E kinetochore motor (7–9).

The Rod–ZW10–Zwilch (RZZ) complex has been reported to be a key player in spindle assembly checkpoint (SAC) activation as it is required to recruit SAC proteins Mad1 and Mad2 to kinetochores in both *Drosophila* and humans (10–15). More importantly, it has also been shown that the RZZ complex is important to recruit dynein to kinetochores through its direct association with the dynein adaptor protein Spindly (16–21). However, it is clear that there are also RZZ-independent mechanisms (such as the CENP-F/NudE pathway) contributing to this function (22, 23). The dynein motor has been shown to be involved in rapid movement of mono-oriented chromosomes toward the spindle poles via dynamic lateral interaction between kinetochores and astral microtubules during early prometaphase, thus contributing to chromosome alignment (2, 21, 24–26). As these proteins are interlinked and function together at kinetochores in this process for maintaining dynamic kMT attachments, they constitute a module referred to as the "dynein module" (27).

The Ndc80 complex, consisting of four coiled-coil proteins, Hec1, Nuf2, Spc24, and Spc25, is a major constituent of the outer plate of kinetochores and is required for stable end-on kMT attachments after chromosome alignment at the metaphase plate (27–29). Recent studies in *Caenorhabditis elegans*

This work was supported by National Institutes of Health NCI Grant R00CA178188 (to D. V.), NINDS Grant R00NS089428 (to R. J. M.), and NIGMS Grant R35GM124889 (to R. J. M.). The authors declare that they have no conflicts of interest with the contents of this article. The content is solely the responsibility of the authors and does not necessarily represent the official views of the National Institutes of Health.

This article contains Figs. S1–S3 and Movies S1–S6.

[1] To whom correspondence should be addressed. E-mail: dileep.varma@northwestern.edu.

[2] The abbreviations used are: NEB, nuclear envelope breakdown; kMT, kinetochore–microtubule; RZZ, Rod–Zw10–Zwilch; SAC, spindle assembly checkpoint; Ndc80, nuclear division cycle 80; CENP, centrosome-associated protein; siRNA, small interfering RNA; KMN, Knl1–Mis12–Ndc80; TIRF, total internal reflection fluorescence; TMR, tetramethylrhodamine; DDB, dynein–dynactin–BicD2; k–k distance, distance between sister kinetochores; IF, immunofluorescence; WB, Western blotting; EMCCD, electron-multiplying charge-coupled device; ROI, region of interest.

have shown that the Rod subunit of the RZZ complex interacts with the Hec1 subunit of the Ndc80 complex and that this association is critical for forming stable kMT attachments during mitotic chromosome alignment. The presence of Rod at kinetochores was shown to be inhibitory for the formation of stable kMT attachments by the Ndc80 complex, possibly in the early stages of mitosis, to control the strength of kMT attachments in an Aurora B kinase–independent manner (17, 27). The removal of SAC proteins, including Rod, from kinetochores by Spindly-dynein–mediated "stripping" during checkpoint silencing is thought to enable Ndc80 to form stable kMT attachments at the spindle equator. In addition, super-resolution mapping of the kinetochore location of the components of the RZZ complex in humans suggests that they are located very proximal to the N-terminal region of the Ndc80 complex (15), which has been established to be critical for stable kMT attachment formation (28, 30–34).

However, whether/how the dynein module regulates kMT attachments of Ndc80 during early mitosis at human kinetochores to drive chromosome motility and alignment is unclear. Here, we address the functional relationship between the dynein module and the Ndc80 complex for chromosome alignment in human cells by using high-resolution confocal microscopy and siRNA-mediated functional perturbation studies. We found that the components of the dynein module regulate the stability of Ndc80-mediated kMT attachments through multiple modes. Although dynein and/or the spindly component serves to relieve the Rod-mediated inhibition of Ndc80, we found that the dynein motor and Ndc80 can also directly influence each other's MT binding to control kMT dynamicity and chromosome alignment.

Results and discussion

Evidence for coordination between the dynein and Ndc80 kinetochore modules for proper chromosome alignment in humans

It is well established that the attachments between kinetochores and kMTs in early mitosis are dynamic in nature to favor kinetochore–MT motor-dependent chromosome motility that drives chromosome congression and to aid in attachment error correction (35). It is also established that the Ndc80 complex at kinetochores forms strong attachments with spindle MTs to stabilize kMT attachments during chromosome alignment and biorientation at the spindle equator in metaphase (36, 37) and that purified Ndc80 binds to microtubules with high affinity *in vitro* (30, 38, 39). Consistent with this, we found that relatively low concentrations of GFP-tagged Hec1/Nuf2 dimer of the Ndc80 complex (1–5 nM) bound readily to Dylight405-labeled MTs immobilized on coverslips in *in vitro* TIRF microscopy assays (Fig. 1*A*). In addition, the Ndc80 complex and the dynein motor share similar binding sites on MTs (40, 41), which points to the notion that Ndc80-mediated kMT attachments may be mutually exclusive with dynein-based attachments during mitosis. We tested this directly by carrying out TIRF microscopy assays using GFP-tagged Hec1/Nuf2 dimer and tetramethylrhodamine (TMR)-labeled dynein–dynactin–BicD2 (DDB) cocomplex (42). We found that the presence of higher concentrations of the Hec1/Nuf2 dimer (20 nM, strongly inhibited the binding of the DDB complex to MTs, supporting this prediction (Fig. 1, *B* and *C*). Consistent with this finding, it has been observed in *Xenopus* cells that the velocity of dynein-based poleward movement was substantially enhanced in the absence of the Ndc80 complex (26).

Our data support the idea that the MT-binding activity of the Ndc80 complex could be directly affected by high local concentrations of dynein at prometaphase kinetochores. We surmise that the initial capture and dynein-dependent poleward motility of kinetochores could thus be a natural bias for attachments that are dynamic in nature and a mechanism that prevents Ndc80-mediated stable attachments during early mitosis. Although our data support the hypothesis that dynein and Ndc80 directly affect each other's MT binding, it is also possible that there are mechanisms like that observed in *C. elegans* involving the components of the dynein module, including Spindly and Rod, that might modulate the function of Ndc80 in humans, and we sought to test this possibility next.

Defects in chromosome alignment induced by Spindly or dynein depletion are rescued by codepletion of Rod

As Spindly has been shown to relieve the inhibition of Ndc80 by Rod to enable the formation of Ndc80-mediated stable kMT attachments in worms (17, 27), we tested whether Rod is functionally related to Spindly in humans as has been observed in worms. We sought to assess the phenotype of chromosome alignment in cells where the function of Rod and/or the dynein anchor Spindly was disrupted by RNA interference (RNAi)–mediated knockdown of both proteins. Efficient depletion of the target proteins was validated by immunoblotting as well as immunostaining analyses (Fig. 1, *D* and *E* and Fig. S1*A*). We found that mitotic cells depleted of Rod (Rod^{siRNA}) exhibit no apparent defect in chromosome alignment at the metaphase plate (Fig. 1*E* and Fig. S1*A*). As observed in worms (17, 27), the severe chromosome misalignment produced by Spindly depletion ($Spindly^{siRNA}$) was rescued by the codepletion of Rod ($Spindly/Rod^{siRNA}$) (Fig. 1, *E* and *F*, and Fig. S1*A*). The frequency of mitotic cells with misaligned chromosomes was significantly lower after $Spindly/Rod^{siRNA}$ compared with that of $Spindly^{siRNA}$ (Fig. 1*F*). These observations suggest that the modulation of Rod function by Spindly to aid in the formation of Ndc80-mediated stable kMT attachments is conserved from worms to humans, but the molecular mechanism of how this inhibition is accomplished is poorly understood.

Because dynein uses Spindly as an adaptor to bind to the RZZ complex and get recruited to kinetochores (17–19), we then tested whether chromosome alignment defects after $dynein^{siRNA}$ are also rescued by codepletion of Rod. To effectively deplete dynein, we designed a new siRNA targeting the 3′-UTR sequence of the *DYNC1H1* gene. Efficient depletion of the target proteins was validated by immunoblotting as well as immunostaining analyses (Fig. 2, *A–C*, and Fig. S1*A*). As expected (21, 24, 43), depletion of dynein caused a significant increase in the percentage of mitotic cells with misaligned chromosomes in HeLa cells (Fig. 2, *C* and *D*). In contrast, the frequency of cells with misaligned chromosomes was significantly reduced after $dynein/Rod^{siRNA}$ compared with that of $dynein^{siRNA}$ and was

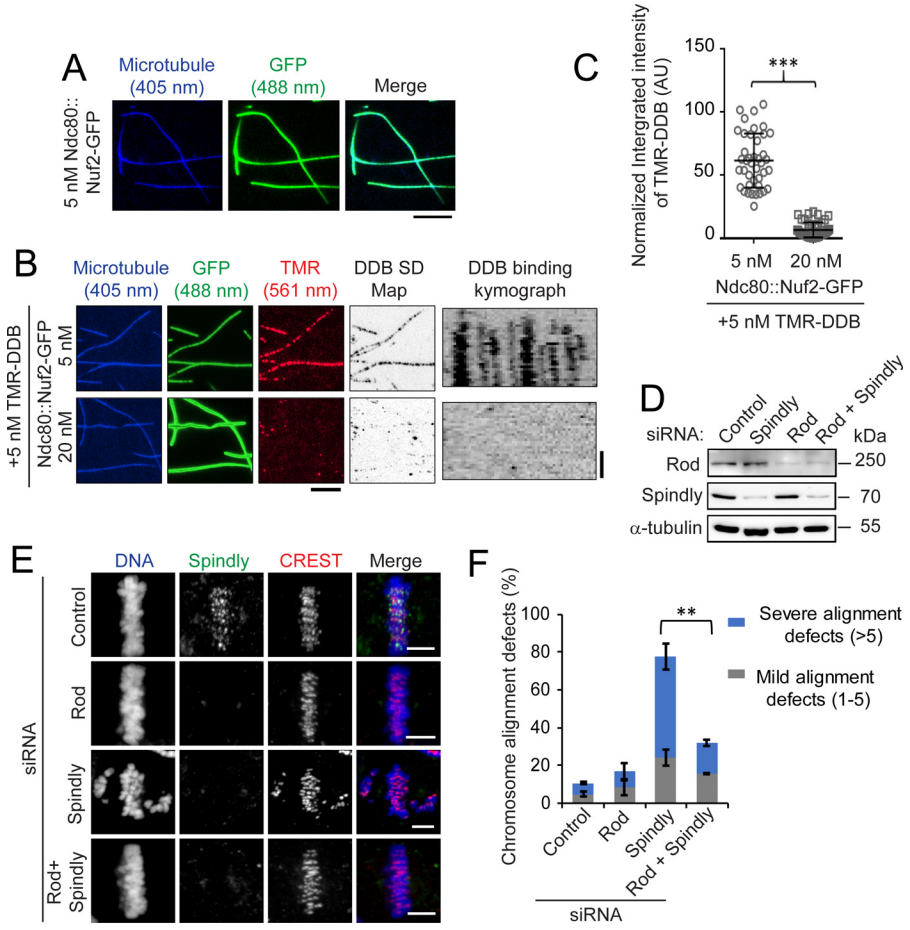

Figure 1. *A–C*, higher concentrations of Ndc80 inhibit dynein–MT binding in *in vitro* TIRF microscopy assays. *A*, representative TIRF microscopy images showing surface-attached Dylight405-labeled MTs (*blue*) and Ndc80::Nuf2-GFP (*green*) at 5 nM. *B*, a higher concentration of Ndc80::Nuf2-GFP (20 nM) (*green*) strongly inhibits the binding of TMR-DDB (*red*) on surface-attached Dylight405-labeled MTs (*blue*). The signal intensity of Ndc80::Nuf2-GFP is scaled identically between images. The image of TMR-DDB (*red*) shown is from the last time frame of the time series. An S.D. map of TMR-DDB binding over a 5-min movie is shown (60) along with a representative kymograph showing TMR-DDB binding on a single MT. In the absence of ATP, TMR-DDB binds statically to the MT lattice (*vertical lines* in kymograph). *Scale bars*, 5 μm, 2 min. *C*, quantification of integrated intensity of TMR-DDB on surface-attached MTs in the presence of variable concentration of Ndc80::Nuf2-GFP. Intensity was measured for at least 25 different locations along MTs for three independent images. *AU*, arbitrary units. ***, $p < 0.005$ (Mann–Whitney *U* test). *D–F*, rescue of chromosome alignment defects of Spindly-depleted cells by codepletion of Rod. *D*, Western blot analysis of HeLa cells treated with siRNAs for control, Spindly, Rod, and Spindly + Rod. α-Tubulin was used as a loading control. *E*, immunofluorescence staining of mitotic cells depleted of target proteins as indicated in comparison with control cells (*top panel*) for Spindly (*green*) and a kinetochore marker (anti-centromere antiserum (*CREST*); *red*) and counterstained with DAPI for DNA. *Scale bars*, 5 μm. *F*, quantification of mitotic cells with chromosome alignment defects in cells from *E*. *Error bars* represent S.D. from three independent experiments. For each experiment, 200 mitotic cells were examined. **, $p < 0.01$ (Student's *t* test).

similar to that of control^{siRNA} (Fig. 2, *C* and *D*, and Fig. S1*A*). As a positive control, depletion of Ndc80 using siRNA-mediated knockdown of the Hec1 subunit (Ndc80^{siRNA}) expectedly led to severe chromosome alignment defects (44, 45) (Fig. 2*D* and Fig. S2, *A* and *B*). We further confirmed the rescue of chromosome alignment defects after dynein/Rod^{siRNA} by live imaging. We found that ~80% of control cells could align their chromosomes at the metaphase plate within 30 min of the NEB, whereas ~75% dynein^{siRNA} cells were not able to do so even 120 min after the NEB. In contrast, ~60% of dynein/Rod^{siRNA} cells could align their chromosomes with only a mild delay compared with control^{siRNA} cells (Fig. 2, *E* and *F*, and Movies S1–S4). As expected, we also observed severe chromosome alignment defects by live-cell imaging after Ndc80^{siRNA} (Fig. 2*F*, Fig. S2*C*, and Movies *S5* and *S6*). Thus, our results suggest that the defect in chromosome alignment resulting from dynein depletion was surprisingly rescued by codepletion of Rod.

The existing paradigm demonstrating a critical role for dynein in the rapid poleward movement of chromosomes during early mitosis to drive chromosome alignment originates from studies in large mitotic cells such as newt pneumocytes where the chromosomes are separated by relatively large distances (10's of μms) from the spindle poles (46). However, in smaller mitotic cells such as HeLa cells, where the chromosomes are separated by much smaller distances from the spindle poles (5–10 μms), we surmise that the disengagement of dynein/Spindly from Rod and Ndc80 is a major cause of chromosome misalignment after dynein or Spindly depletion, due to which Rod is able to impart a sustained inhibition of Ndc80 function. It is also possible that the polar ejection forces on chromosome arms produced by the MT plus-end–directed chromokinesin motors drive the chromosomes away from the spindle poles during early mitosis in the absence of dynein or Spindly to hinder proper chromosome alignment (4, 47) (also see Fig. 3).

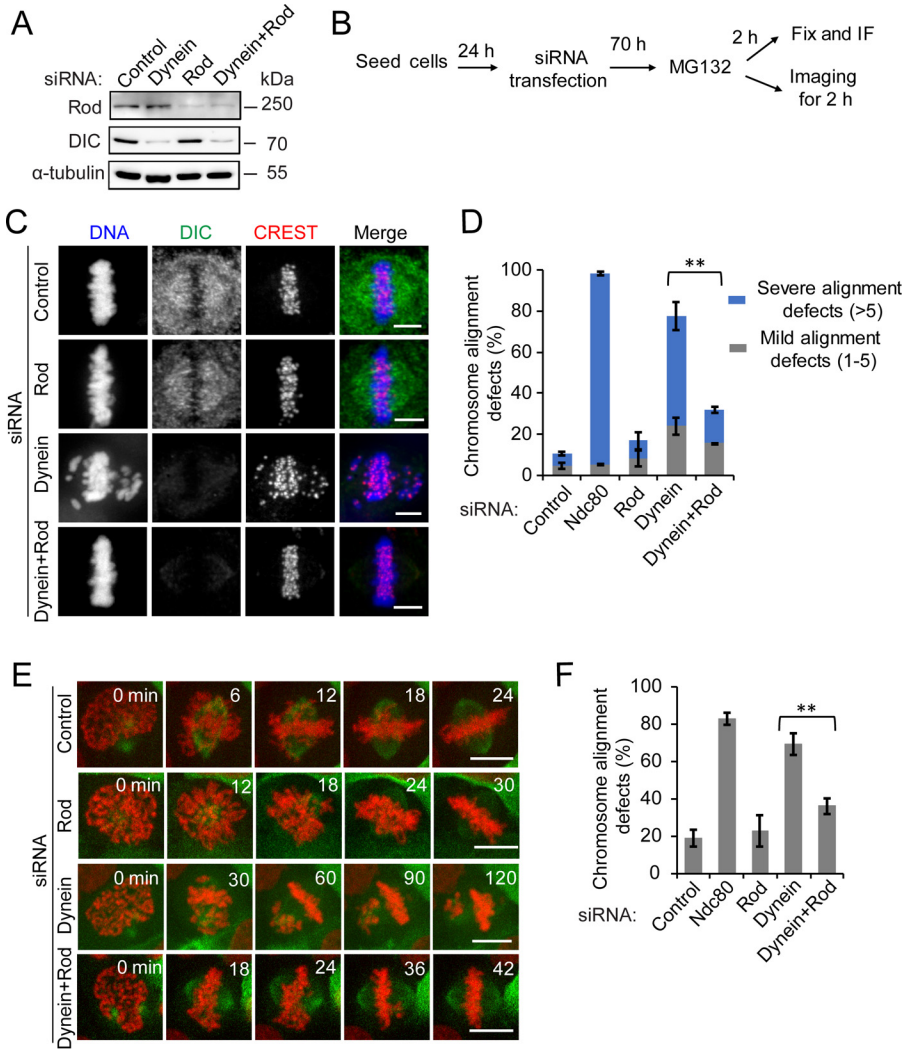

Figure 2. Rod codepletion rescues the defects in chromosome alignment induced by depletion of dynein. *A*, Western blot analysis of HeLa cells treated with siRNAs for control, dynein, Rod, and dynein + Rod. α-Tubulin was used as a loading control. *B*, cells were transfected with the indicated siRNAs, synchronized, and fixed according to the scheme. *C*, immunofluorescence staining of mitotic cells depleted of target proteins as indicated in comparison with control cells (*top panel*) for dynein intermediate chain (*DIC*; *green*) and a kinetochore marker (anti-centromere antiserum (*CREST*); *red*) and counterstained with DAPI for DNA. *Scale bars*, 5 μm. *D*, quantification of mitotic cells with chromosome alignment defects in cells from *C* and in cells depleted of Ndc80 (also see Fig. S2). *Error bars* represent S.D. from three independent experiments. For each experiment, 200 mitotic cells were examined. **, $p < 0.01$ (Student's *t* test). *E*, selected frames of videos from HeLa cells expressing H2B-mCherry and GFP-α-tubulin treated with siRNAs as indicated. Images were captured at 6-min intervals starting from nuclear envelope breakdown for 2 h immediately after the addition of MG132. *Scale bars*, 10 μm. *F*, quantification of cells with chromosome alignment defects in *E* and of cells with chromosome alignment defects after Ndc80 depletion (also see Fig. S2). *Error bars* represent S.D. from three independent experiments. For each experiment, 30 mitotic cells were examined. **, $p < 0.01$ (Student's *t* test).

The restoration of proper chromosome alignment in Rod-depleted cells is independent of its function in the spindle assembly checkpoint activation

The RZZ complex is important to recruit the SAC proteins Mad1 and Mad2 to kinetochores in both *Drosophila* and humans (10–15). To scrutinize the possibility that the rescue of chromosome alignment after dynein/Rod^{siRNA} was not due to aberrant checkpoint silencing, we tested the recruitment of SAC protein Mad1 to kinetochores of mitotic cells in prometaphase. We found that detectable levels of Mad1 persisted at kinetochores in prometaphase cells depleted of Rod, dynein, or both Rod and dynein (Fig. S1*B*). When we analyzed mitotic progression by live imaging, we found no apparent defect in chromosome alignment at the metaphase plate after dynein/Rod^{siRNA} similar to that of Rod^{siRNA} (Fig. 2, *E* and *F*). Moreover, in both cases, live cells that were not treated with MG132 neither underwent premature anaphase onset during mitosis nor exhibited formation of micronuclei in interphase (data not depicted), implying that the function of Rod in chromosome alignment could be independent of its role in SAC activation during mitosis in human cells. These data also suggest that dynein/Rod^{siRNA} cells can align their chromosomes properly without impairing checkpoint activation.

The rescue of chromosome alignment defects after dynein and Rod codepletion is accompanied by restoration of attachment and stability of kMT

Proper chromosome alignment at the metaphase plate is accompanied by the stabilization of kMTs, which are MT bundles that extend from the bioriented kinetochores to spindle

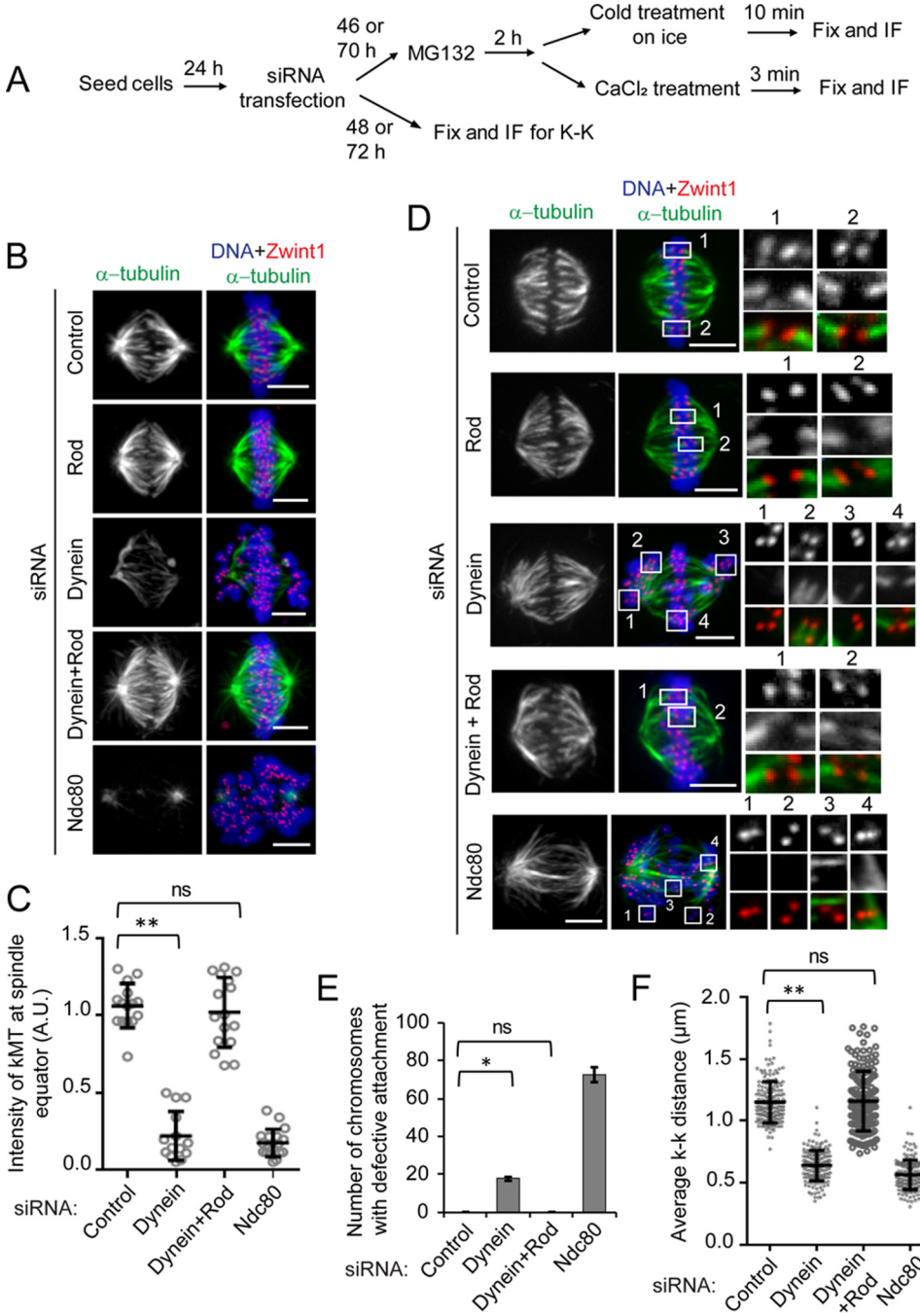

Figure 3. The formation of stable kMT attachments in dynein-depleted cells is restored by codepletion of Rod. *A*, cells were transfected with the indicated siRNAs, synchronized, cold-treated, and fixed according to the scheme. *B*, HeLa cells treated with siRNAs as indicated after cold treatment were immunostained for α-tubulin (*green*) and Zwint1 as a kinetochore marker (*red*) and counterstained with DAPI for DNA (*blue*). *Scale bars*, 5 μm. *C*, quantification of intensities of cold-stable kMTs at the spindle equator of metaphase plate in *B*. *A.U.*, arbitrary units. *Error bars* represent S.D. from three independent experiments. For each experiment, 10 cells were examined. **, $p < 0.01$ (Mann–Whitney *U* test); *ns*, not significant. *D*, analysis of end-on kMT attachments and kinetochore biorientation in cells treated with siRNAs as indicated. Cells were pretreated with $CaCl_2$ (0.2 mM) for 3 min to depolymerize unstable microtubules, immunostained for α-tubulin (*green*) and Zwint1 as a kinetochore marker (*red*), and counterstained with DAPI for DNA (*blue*). *Scale bars*, 5 μm. *E*, quantification of the number of chromosomes with defective kMT attachments in *D*. *Error bars* represent S.D. from three independent experiments. For each experiment, 10 cells were examined. *, $p < 0.05$ (Student's *t* test); *ns*, not significant. *F*, quantification of interkinetochore (k–k) distances measured from Zwint1 signals at sister kinetochore pairs of cells treated with siRNAs as indicated. *Error bars* represent S.D. from three independent experiments. For each experiment, 10 cells were examined. Distance was measured for at least 10 pairs of kinetochores from each cell. $n = 150$. **, $p < 0.01$ (Mann–Whitney *U* test); *ns*, not significant.

poles (48–50). Our immunostaining data showed that kMTs resistant to cold treatment were markedly reduced in mitotic cells after dynein^{siRNA} as compared with those of control^{siRNA} (Fig. 3, *A*–*C*). Surprisingly, we found that dynein/Rod^{siRNA} cells were able to form robust kMTs to a similar extent as was observed after control^{siRNA} or Rod^{siRNA} (Fig. 3, *B* and *C*). As a positive control, we observed a severe lack of cold-stable kMTs after Ndc80^{siRNA} (Fig. 3, *B* and *C*). These data suggest that Rod's inhibition of Ndc80-mediated kMT attachments (27) is promoted in the absence of the counteractivity of dynein on Rod; as

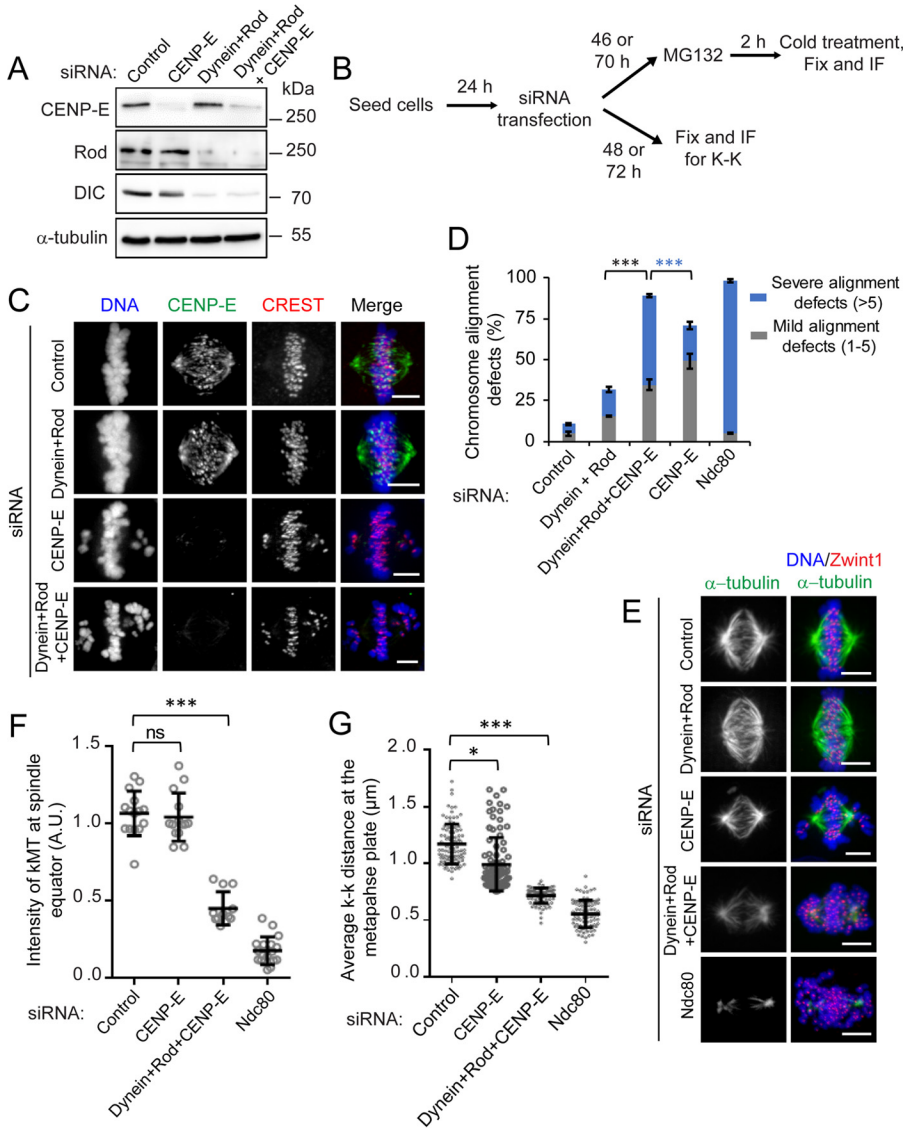

Figure 4. Chromosome alignment in cells codepleted of dynein and Rod is dependent on the motor activity of CENP-E. *A*, Western blot analysis of HeLa cells treated with siRNAs for control, CENP-E, dynein + Rod, and dynein + Rod + CENP-E. α-Tubulin was used as a loading control. *B*, cells were transfected with the indicated siRNAs, synchronized, cold-treated, and fixed according to the scheme. *C*, immunofluorescence staining of mitotic cells depleted of target proteins as indicated in comparison with control cells (*top panel*) for CENP-E (*green*) and a kinetochore marker (anti-centromere antiserum (*CREST*); *red*) and counterstained with DAPI for DNA (*blue*). *Scale bars*, 5 μm. *D*, quantification of mitotic cells with chromosome alignment defects in cells from *C* and for cells treated with siRNA for Ndc80. *Error bars* represent S.D. from three independent experiments. For each experiment, 200 mitotic cells were examined. ***, $p < 0.005$ (Student's *t* test). *E*, HeLa cells treated with ice-cold L-15 medium after treatment with siRNAs as indicated were immunostained for spindle MT (*green*) and a kinetochore marker (Zwint1; *red*) and counterstained with DAPI for DNA (*blue*). *Scale bars*, 5 μm. *F*, quantification of intensities of kMTs adjacent to the kMT attachment sites. *A.U.*, arbitrary units. *Error bars* represent S.D. from the mean for three independent experiments. For each experiment, 10 cells were examined. ***, $p < 0.005$ (Mann–Whitney *U* test); *ns*, not significant. *G*, quantification of interkinetochore (k–k) distances measured from Zwint1 signals at kinetochore pairs of cells treated with the siRNAs indicated. *Error bars* represent S.D. from three independent experiments. For each experiment, 10 cells were examined. Distance was measured for at least 10 pairs of kinetochores from each cell. ***, $p < 0.005$; *, $p < 0.05$ (Mann–Whitney *U* test).

a consequence, kMT attachments are unstable in dynein-depleted cells.

Analyses of kMT attachments in cells treated with 0.2 mM $CaCl_2$ followed by immunostaining showed that dynein^{siRNA} caused misaligned chromosomes with syntelic, monotelic, and unattached kMT attachments (Fig. 3, *D* and *E*). In the absence of the poleward-directed motor activity of dynein, we surmise that the misaligned chromosomes are driven to form syntelic and monotelic kMT attachments due to the activity of plus-end–directed chromokinesin motors (4, 47). We found that these defects in kMT attachments resulting from dynein depletion were rescued by codepletion of Rod. The number of defective kMT attachments was significantly lower after dynein/Rod^{siRNA} compared with that of dynein^{siRNA} and was similar to that of control^{siRNA} (Fig. 3, *D* and *E*). To further assess kMT attachment stability, we measured the distances between sister kinetochores (k–k distances) of bioriented chromosomes at the spindle equator. Stable attachments of sister kinetochore pairs to spindle MTs emanating from opposite spindle poles generate stretch between them that can be measured by the k–k distance. The reduction in average k–k distance in cells after dynein^{siRNA} cells was rescued by codepletion of Rod and was similar to control^{siRNA} (Fig. 3, *D* and *F*), possibly due to the re-establishment of stable kMT attachments that we observed.

Thus, we found that the defects in generating kinetochore stretch on bioriented chromosomes resulting from dynein depletion were rescued by codepletion of Rod. As a positive control, Ndc80^{siRNA} cells exhibited severely defective kMT attachments and abnormal interkinetochore stretch (44, 51) (Fig. 3, *D* and *E*). These results suggested that codepletion of Rod rescued the defects in chromosome alignment resulting from dynein depletion by restoring the robustness of kMTs, stability of kMT attachments, and average interkinetochore distances.

We hypothesize that during early mitosis, in the absence of the kinetochore dynein module, Ndc80 plays a role in the formation of initial kMT attachments, which are subsequently stabilized after chromosome alignment at the metaphase plate driven by CENP-E and/or chromokinesins. To support this prediction, we tested the status of kMT attachment of misaligned chromosomes in cells depleted of dynein or Ndc80. Close inspection of misaligned chromosomes showed that kinetochores were attached to MTs with syntelic or monotelic orientation after dynein^{siRNA}, whereas those in Ndc80^{siRNA} cells remained unattached (Fig. 3*D*), suggesting that Ndc80 might have an unexplored, but important role in initial kMT capture. These observations could also explain how chromosomes are still captured by spindle MTs after dynein/Rod^{siRNA}. These results support the idea that a key function of Rod is to inhibit Ndc80 because kMT attachments are rescued when Rod is codepleted with either Spindly (17, 27, 52) or dynein (this study).

Together, these data suggest that Rod is a negative regulator of stable kMT attachments and serves to perturb the function of the Ndc80 complex (27) but also that its inhibitory function is controlled by Spindly and dynein, the mechanism for which is yet unclear. The above data also suggest that chromosome alignment can be achieved at the spindle equator in the absence of the dynein module for human kinetochores when normal chromosome alignment could possibly occur either by the activity of residual CENP-F/NudE–recruited dynein (22, 23) and/or by the activity of the plus-end–directed kinetochore motor CENP-E.

Chromosome alignment in cells codepleted of dynein and Rod is dependent on the motor activity of CENP-E

As normal chromosome alignment persists after dynein/Rod^{siRNA}, we sought to investigate whether the plus-end–directed kinetochore motor CENP-E, which is involved in transporting unattached sister kinetochores along pre-existing microtubule bundles to the metaphase plate (4, 8, 53, 54), was involved in chromosome congression by simultaneously perturbing CENP-E function using siRNA-mediated knockdown in dynein/Rod^{siRNA} cells. Efficient depletion of the target proteins was validated by immunoblotting as well as immunostaining analyses (Fig. 4, *A* and *C*, and Fig. S3, *A* and *B*). Immunostaining data showed that the frequency of cells with severe chromosome misalignment (more than five chromosomes) was significantly higher after dynein/Rod/CENP-E^{siRNA} (~54%) as compared with that after control^{siRNA} (~5%), dynein/Rod^{siRNA} (~16%), or CENP-E^{siRNA} (~21%) (Fig. 4, *C* and *D*, and Fig. S3, *A* and *B*). As a positive control described previously, ~80% of cells

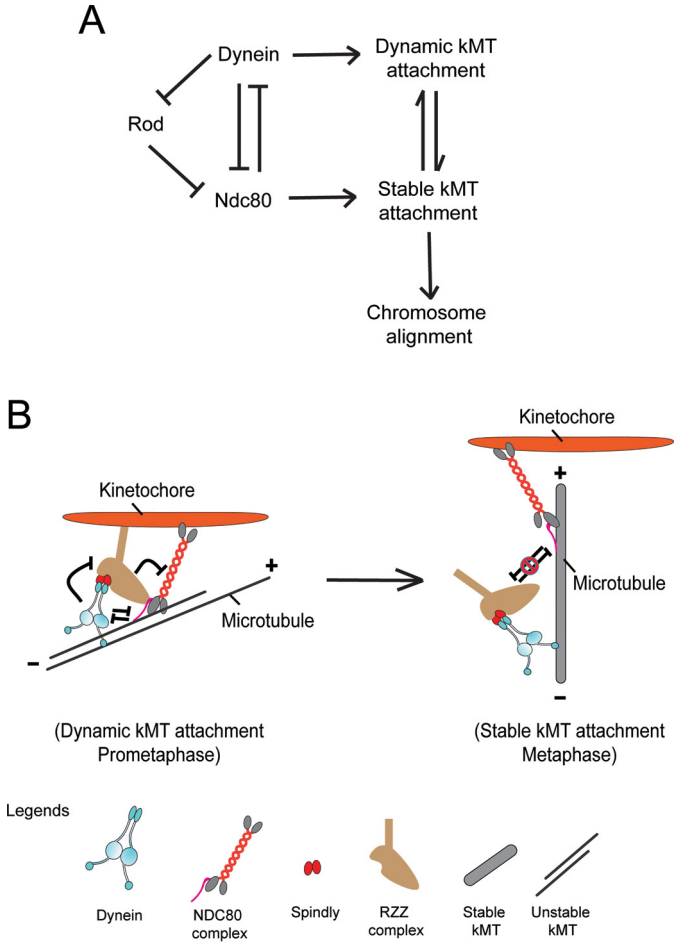

Figure 5. *A*, a model integrating the mechanisms that control stable kMT attachments in humans. During early mitosis, Rod, a subunit of the RZZ complex, which is involved in the recruitment of both dynein and its adaptor Spindly, inhibits Ndc80 to prevent the formation of premature stable kMT attachments. Dynein and Spindly, which are involved in dynamic kMT attachments, inhibit Rod by a yet unclear mechanism to modulate Rod-mediated inhibition of Ndc80 in stabilizing kMT attachments. Ndc80 can directly inhibit dynein binding to MTs while higher levels of dynein at prometaphase kinetochores might reciprocally also interfere with Ndc80–MT binding. Thus, dynein-mediated dynamic kMT attachments and Ndc80-mediated stable kMT attachments are coordinated during early mitosis either by a direct interplay between dynein and Ndc80 and/or by the mediation of Rod to drive proper chromosome alignment. *B*, a schematic representation of the key players including dynein, RZZ, and Ndc80 and their hypothesized roles in the maturation of kMT attachments from a dynamic state in prometaphase to a stable state in metaphase as described in the model in *A*.

after Ndc80^{siRNA} exhibited major chromosome misalignments (Fig. S2, *A* and *B*). We further confirmed this result by inhibiting the motor activity of CENP-E using the small molecule inhibitor GSK-923295 (55), which we found also abolished the rescue of chromosome alignment defects after dynein/Rod^{siRNA} (Fig. S3, *C–E*).

The lack of rescue of chromosome alignment after dynein/Rod/CENP-E^{siRNA} prompted us to test whether stable kMT attachments were formed normally in these cells. We observed a substantial decrease in the intensity of kMTs at the spindle equator after dynein/Rod/CENP-E^{siRNA} similar to that of Ndc80^{siRNA} (Fig. 4, *E* and *F*) and in contrast to what was previously observed after dynein/Rod^{siRNA} or CENP-E^{siRNA} (Figs. 3, *B* and *C*, and 4, *E* and *F*). We posit that the severe chromosome misalignment produced after dynein/Rod/CENP-E^{siRNA} prevents proper kinetochore

biorientation due to which the kMTs retain their cold-sensitive nature. Moreover, the average interkinetochore distance was significantly reduced after dynein/Rod/CENP-E^{siRNA} in contrast to that of control^{siRNA} or CENP-E^{siRNA} and similar to that of Ndc80^{siRNA} (Fig. 4*G*). These observations suggest a biased mechanism for the rescue of chromosome alignment after dynein/Rod^{siRNA} that is mediated by the plus-end–directed motility of CENP-E.

Summary and conclusions

Overall, this study establishes a functional relationship between the kinetochore dynein module and Ndc80 module for proper chromosome alignment in humans. Rod is a key recruiter of the dynein module because it is involved in recruiting both dynein and Spindly to kinetochores (16, 18, 19, 52, 56). Our experimental results show that depletion of Rod alone has no apparent effect on chromosome alignment (Fig. 1, *E* and *F*). We found that severe defects of chromosome alignment after Spindly^{siRNA} were rescued by codepletion of Rod in humans similarly to observations in worms (17, 27). Surprisingly, we also found that severe defects in chromosome alignment after dynein^{siRNA} were rescued by codepletion of Rod. As Spindly, a dynein adapter, counteracts the inhibitory role of Rod in the formation of Ndc80-mediated stable end-on kMT attachments (17, 27), the analogous relationship between dynein and Rod, like that of Spindly and Rod, led us to propose that dynein could also directly counteract the inhibitory role of Rod on stable kMT attachments during early mitosis. Therefore, the phenotypes of either Spindly^{siRNA} or dynein^{siRNA} represent the outcome of the disengagement of Rod from these factors, thus leading to severe chromosome alignment defects. Taken together, these observations led us to conclude that the role of the dynein module in chromosome alignment depends on the function of Rod. It is not clear at this point whether it is the Rod/Spindly–dependent or CENP-F/NudE–dependent kinetochore dynein population that is critical for the dynein-module mediated control of Ndc80 function in early mitosis.

Under normal condition after the NEB, kinetochores that are initially attached to spindle MTs by the search and capture mechanism are rapidly transported poleward along MTs primarily by the minus-end–directed motor force of dynein, and consequently chromosomes congress to the spindle equator by the activity of CENP-E motor (4). From recent studies (Refs. 17 and 27 and this study), we propose a refined model for controlling kMT attachments during early mitosis in human cells where Spindly inhibits Rod directly and/or through the dynein motor. Initial kMT attachments can still be formed by Ndc80 but are not stabilized due to antagonistic activity between the dynein module and Ndc80 (Fig. 5, *A* and *B*; details in legend). However, the precise mechanism for how Spindly/dynein interferes with Rod function and how Rod inhibits Ndc80 is still unclear. The initial kMT attachments allow dynein-mediated transport of chromosomes to the spindle pole in early mitosis during which both CENP-E activity and end-on attachment formation are expected not to be favored (7). Therefore, in cells codepleted of dynein and Rod during early mitosis, initial kMT attachments can be formed by Ndc80, and chromosomes can be transported poleward by shrinkage of peripheral MT bundles followed by congression at the metaphase plate mediated by CENP-E activity. Our current data led us to propose the existence of two possibly interconnected mechanisms to control the stability of kMT attachments by the Ndc80 complex. Dynein might inhibit Rod to aid in Ndc80-mediated initial kMT attachments while at the same time or in an independent manner directly inhibit the binding of the Ndc80 complex to MTs to prevent premature kMT attachment stabilization during early mitosis.

Another important point to be noted is the conservation of the functional coordination between the dynein module and the Ndc80 complex across different model systems. Considering the studies to date in worms and humans and that the components of the dynein module and Ndc80 are evolutionarily conserved in *C. elegans*, *Drosophila*, and humans (17, 18, 20, 27, 52), it is reasonable to deduce that the above described modes of controlling Ndc80-mediated stable kMT attachment formation by the dynein module are conserved across diverse phyla. Conversely, it is unlikely that these mechanisms exist in budding and fission yeast because the RZZ complex is not conserved and because dynein, although being essential for proper spindle orientation (57), has not been reported to be critical for kinetochore functions in yeast. Moreover, direct antagonism between dynein and Ndc80 is unlikely to broadly impact MT-related cellular functions in yeast as their MT binding is important for functions that are mutually unrelated.

It is becoming clear that stable kMT attachments are regulated not only by components within the dynein module but also by a direct interplay between the dynein module and the Ndc80 complex to prevent premature kMT stabilization. Thus, our results reveal a further layer of the elaborate network involving these distinct modules that are under tight spatiotemporal regulation to control kMT attachments and drive proper chromosome alignment at the metaphase plate. It will be important to continue studying the relationship between these modules and with the protein complexes at the plus-ends of MTs to understand how they might coordinate the events involved in the formation and maturation of kMT attachments during chromosome alignment and segregation.

Materials and methods

Cell culture, transfections, and drug treatments

HeLa cells were grown in Dulbecco's modified Eagle's medium (DMEM; Life Technologies) supplemented with 10% fetal bovine serum at 37 °C in a humidified atmosphere with 5% CO_2. For RNAi experiments, cells were transfected at 30–50% confluence using Dharmafect 2 (Dharmacon) according to the manufacturer's instructions and analyzed 48–72 h after transfection. For rescue experiments, RNAi-refractory constructs were transfected into cells with Lipofectamine 3000 (Life Technologies) for 12 h followed by siRNA transfection. Cells were prepared for analysis after 48 h of siRNA transfection.

To arrest cells at metaphase, cells were treated with MG132 (10 μM) for 2 h prior to fixation. To inhibit CENP-E, 200 nM GSK-923295 (APExBio) was added to the medium, and cells were fixed after 2 h of incubation.

siRNAs targeting cDNAs for Ndc80 (5′-GUUCAAAAG-CUGGAUGAUCdTdT-3′) (45), Rod Invitrogen Stealth (5′-GGAAUGAUAUUGAGCUGCUAACAAA-3′) (58), and CENP-E Invitrogen Stealth (5′-UUAUAUUACAGCCUUC-CUGAGCCG-3′) (59) were used in this study. An siRNA sequence targeting the 3′-UTR of dynein (5′-GGUGGAAAU-UGGAAGGAUAdTdT-3′) was also used (Invitrogen). The SMARTpool ON-TARGETplus siRNAs used for targeting Spindly were purchased from Dharmacon (5′-GGGAGAA-GUUUAUCGAUUA-3′ and 5′-GAAAGGGUCUCAAACU-GAA-3′, 5′-GGAUAAAUGUCGUAAUGAA-3′, and 5′-CAG-GUUAGCUGUUGAAUCA-3′). All siRNAs were used at 100 nM concentration except for dynein, which was used at 200 nM.

Antibodies

The primary monoclonal mouse antibodies used were: anti-Hec1 9G3 (Abcam, ab3613) for IF at 1:400 and WB at 1:1000; anti-dynein clone 74.1 (EMD Millipore, MAB1618) for IF at 1:300 and WB at 1:1000, anti-Rod clone 10H4 (Abnova, H00009735-M01) for IF at 1:300 and WB at 1:1000, anti-CENP-E 1H12 (Abcam, ab5093) for IF at 1:400, and anti-α-tubulin DM1A (Santa Cruz Biotechnology, Sc32293) for IF at 1:750 and WB at 1:1000. The primary rabbit polyclonal antibodies used were: anti-α-tubulin (Abcam, ab18251) for IF at 1:750, anti-Zwint1 (Bethyl Laboratories, A300-781A) for IF at 1:400, anti-Spindly (a gift from Dr. Arshad Desai, University of California, San Diego) for IF at 1:5000, anti-Spindly (Bethyl Laboratories, A301-354AT) for WB at 1:1000, and anti-CENP-E (Bethyl Laboratories, A301-943A) for WB at 1:1000. We also used a human anti-centromere (Immunovision) at 1:1000 for IF.

Immunofluorescence

HeLa cells grown on a glass coverslip were fixed in cold methanol (−20 °C) or 4% formaldehyde after pre-extraction with 0.1% Triton X-100 followed by blocking with 3% bovine serum albumin (BSA) in PBS and incubated with primary antibodies for 1 h at 37 °C followed by washing with PBS (137 mM NaCl, 2.7 mM KCl, 10 mM Na_2HPO_4, and 1.8 mM KH_2PO_4, pH 7.4) supplemented with 0.02% Triton X-100. The primary antibodies were detected using secondary antibodies coupled with Alexa Fluor-488/647 or Rhodamine Red-X (Jackson ImmunoResearch Laboratories) at a dilution of 1:250, and DNA was counterstained with 1 mg/ml DAPI.

For the analysis of cold-stable microtubules, cells were incubated for 10 min on ice in Leibovitz's L-15 medium (Gibco) supplemented with 20 mM HEPES, pH 7.0, and 10% FBS and then fixed for 15 min with 4% formaldehyde in PBS at 37 °C. For the analysis of $CaCl_2$-resistant microtubules, cells were treated with PCM buffer (60 mM PIPES, 0.2 mM $CaCl_2$, and 4 mM $MgSO_4$, pH 6.9) for 3 min and then fixed for 15 min at room temperature with 4% formaldehyde and 0.5% Triton X-100 in PCM buffer.

Image acquisition and analysis

For image acquisition, three-dimensional stacks were obtained through the cell using a Nikon Eclipse TiE inverted microscope equipped with a Yokogawa CSU-X1 spinning disc, an Andor iXon Ultra888 EMCCD camera, and an ×60 or ×100 1.4 numerical aperture Plan-Apochromatic differential interference contrast oil immersion objective (Nikon). For fixed cell experiments, images were acquired at room temperature as z-stacks at 0.2-μm intervals controlled by NIS-Elements software (Nikon). Images were processed in Fiji ImageJ and Adobe Photoshop CC 2015 and represent maximum-intensity projections of the required z-stacks. To measure the fluorescence intensity, we manually selected and measured individual kinetochores by quantification of the pixel gray levels of the focused z-plane in a region of interest (ROI) using Fiji ImageJ. The final intensity was obtained after subtracting the background, which was measured outside of the ROI, from the integrated intensity for the experiment. For the measurement of K-fiber intensity, we converted identically scaled images into TIFF files, selected ROIs at the equatorial position of the metaphase plate, and measured microtubule intensity as described above.

Live-cell imaging

HeLa cells stably expressing mCherry H2B and GFP-α-tubulin or only GFP-H2B were cultured in 35-mm glass-bottomed dishes (MatTek Corp.). Before 30 min of imaging, cell culture medium was changed to prewarmed L-15 medium supplemented with 20% fetal bovine serum and 20 mM HEPES, pH 7.0. Live experiments were carried out in an incubation chamber for microscopes (Tokai Hit Co., Ltd.) at 37 °C in 5% CO_2. Image recording was started immediately after adding MG132 (unless otherwise stated) using an ×60 1.4 numerical aperture Plan-Apochromatic differential interference contrast oil immersion objective mounted on an inverted microscope (Nikon) equipped with an Andor iXon Ultra888 EMCCD camera or an Andor Zyla 4.2 PLUS scientific complementary metal-oxide semiconductor camera. Twelve 1.2-μm–separated z-planes covering the entire volume of the cell were collected every 10 min up to 12 h. Images were processed in Fiji ImageJ and Adobe Photoshop CC 2015 and represent maximum-intensity projections of the required z-stacks.

TIRF microscopy

All imaging experiments were performed at room temperature using a Nikon Eclipse TiE microscope, equipped with a ×100 1.49 numerical aperture oil immersion objective and 1.5× tube lens (yielding a pixel size of 106 nm), an Andor iXon EMCCD camera, and four laser lines (405, 491, 568, and 647 nm), and Micro-Manager 1.4.22 software. Flow chambers containing immobilized microtubules were assembled as described previously (42). All assays were performed in an assay buffer (90 mM HEPES, pH 7.4, 50 mM potassium acetate, 2 mM magnesium acetate, 1 mM EGTA, and 10% glycerol) supplemented with 0.1 mg/ml biotin-BSA, 0.5% Pluronic F-168, and 0.2 mg/ml κ-casein. TMR-labeled DDB and Ndc80::Nuf2-GFP proteins were mixed together and flowed into the chamber, and binding events were imaged over a period of 5 min. For the measurement of DDB intensity on the MT lattice, we converted identically scaled images into TIFF files, selected the ROI on the MT lattice, and obtained final DDB intensity by subtracting the background intensity measured outside of the ROI from the

integrated DDB using FIJI/ImageJ. To generate a standard deviation (S.D.) map of DDB binding, the S.D. projection option was selected within the Z-project tool in Fiji (60).

Immunoprecipitation and immunoblotting

Cell lysates were prepared with lysis buffer (150 mM KCl, 75 mM HEPES, pH 7.5, 1.5 mM EGTA, 1.5 mM $MgCl_2$, 10% glycerol, 0.1% Nonidet P-40, 30 mg/ml DNase, 30 mg/ml RNase, cOmplete protease inhibitor mixture (Roche Applied Science), and complete phosphatase inhibitor mixture (Sigma)). The protein concentration of cell lysate was measured using the Coomassie protein assay kit (Thermo Scientific). For immunoprecipitation assays, precleared native protein extracts (1 mg of total protein) were incubated overnight with mouse anti-dynein clone 74.1 (MAB1618) at a dilution of 1:100 or mouse nonspecific IgG at a dilution of 1:100 (Invitrogen) followed by incubation with 40 μl of anti-mouse-IgG magnetic Dynabeads (Invitrogen) for 2 h at 4 °C. After washing three times with lysis buffer and once with cold 1× TBS-Tween 20, precipitated proteins were eluted by boiling for 5 min in 6× SDS sample buffer. Proteins were separated by SDS-PAGE, electroblotted onto a nitrocellulose blotting membrane (GE Healthcare), and subjected to immunodetection using appropriate primary antibodies. Blocking and antibody incubations were performed in 5% nonfat dry milk. Proteins were visualized using horseradish peroxidase–conjugated secondary antibodies diluted at 1:2000 (Amersham Biosciences) and the ECL system according to the manufacturer's instructions (Thermo Scientific).

Statistical analysis

Mann–Whitney *U* test was used for comparison of dispersion, and a two-sided *t* test was used for comparison of average. The statistical analyses were done with Prism software (GraphPad). Samples for analysis in each data set were acquired in the same experiment, and all samples were calculated at the same time for each data set.

Author contributions—M. A. A. and D. V. conceptualization; M. A. A. data curation; M. A. A. formal analysis; M. A. A. validation; M. A. A. and R. J. M. investigation; M. A. A. and R. J. M. visualization; M. A. A., R. J. M., and D. V. methodology; M. A. A. and D. V. writing-original draft; M. A. A., R. J. M., and D. V. writing-review and editing; D. V. resources; D. V. supervision; D. V. funding acquisition; D. V. project administration.

Acknowledgments—We thank Dhanya Cheerambathur and Arshad Desai for providing Ndc80 (Hec1)::Nuf2-GFP dimeric proteins of the Ndc80 complex.

References

1. Walczak, C. E., Cai, S., and Khodjakov, A. (2010) Mechanisms of chromosome behaviour during mitosis. *Nat. Rev. Mol. Cell Biol.* **11,** 91–102 CrossRef Medline
2. Rieder, C. L., and Salmon, E. D. (1998) The vertebrate cell kinetochore and its roles during mitosis. *Trends Cell Biol.* **8,** 310–318 CrossRef Medline
3. Mitchison, T., Evans, L., Schulze, E., and Kirschner, M. (1986) Sites of microtubule assembly and disassembly in the mitotic spindle. *Cell* **45,** 515–527 CrossRef Medline
4. Barisic, M., Aguiar, P., Geley, S., and Maiato, H. (2014) Kinetochore motors drive congression of peripheral polar chromosomes by overcoming random arm-ejection forces. *Nat. Cell Biol.* **16,** 1249–1256 CrossRef Medline
5. Cross, R. A., and McAinsh, A. (2014) Prime movers: the mechanochemistry of mitotic kinesins. *Nat. Rev. Mol. Cell Biol.* **15,** 257–271 CrossRef Medline
6. McIntosh, J. R., Molodtsov, M. I., and Ataullakhanov, F. I. (2012) Biophysics of mitosis. *Q. Rev. Biophys.* **45,** 147–207 CrossRef Medline
7. Barisic, M., and Maiato, H. (2016) The tubulin code: a navigation system for chromosomes during mitosis. *Trends Cell Biol.* **26,** 766–775 CrossRef Medline
8. Kapoor, T. M., Lampson, M. A., Hergert, P., Cameron, L., Cimini, D., Salmon, E. D., McEwen, B. F., and Khodjakov, A. (2006) Chromosomes can congress to the metaphase plate before biorientation. *Science* **311,** 388–391 CrossRef Medline
9. Kim, Y., Heuser, J. E., Waterman, C. M., and Cleveland, D. W. (2008) CENP-E combines a slow, processive motor and a flexible coiled coil to produce an essential motile kinetochore tether. *J. Cell Biol.* **181,** 411–419 CrossRef Medline
10. Buffin, E., Lefebvre, C., Huang, J., Gagou, M. E., and Karess, R. E. (2005) Recruitment of Mad2 to the kinetochore requires the Rod/Zw10 complex. *Curr. Biol.* **15,** 856–861 CrossRef Medline
11. Caldas, G. V., Lynch, T. R., Anderson, R., Afreen, S., Varma, D., and DeLuca, J. G. (2015) The RZZ complex requires the N-terminus of KNL1 to mediate optimal Mad1 kinetochore localization in human cells. *Open Biol.* **5,** 150160 CrossRef Medline
12. Karess, R. (2005) Rod-Zw10-Zwilch: a key player in the spindle checkpoint. *Trends Cell Biol.* **15,** 386–392 CrossRef Medline
13. Kops, G. J., Kim, Y., Weaver, B. A., Mao, Y., McLeod, I., Yates, J. R., 3rd, Tagaya, M., and Cleveland, D. W. (2005) ZW10 links mitotic checkpoint signaling to the structural kinetochore. *J. Cell Biol.* **169,** 49–60 CrossRef Medline
14. Starr, D. A., Williams, B. C., Li, Z., Etemad-Moghadam, B., Dawe, R. K., and Goldberg, M. L. (1997) Conservation of the centromere/kinetochore protein ZW10. *J. Cell Biol.* **138,** 1289–1301 CrossRef Medline
15. Varma, D., Wan, X., Cheerambathur, D., Gassmann, R., Suzuki, A., Lawrimore, J., Desai, A., and Salmon, E. D. (2013) Spindle assembly checkpoint proteins are positioned close to core microtubule attachment sites at kinetochores. *J. Cell Biol.* **202,** 735–746 CrossRef Medline
16. Chan, Y. W., Fava, L. L., Uldschmid, A., Schmitz, M. H., Gerlich, D. W., Nigg, E. A., and Santamaria, A. (2009) Mitotic control of kinetochore-associated dynein and spindle orientation by human Spindly. *J. Cell Biol.* **185,** 859–874 CrossRef Medline
17. Gassmann, R., Essex, A., Hu, J. S., Maddox, P. S., Motegi, F., Sugimoto, A., O'Rourke, S. M., Bowerman, B., McLeod, I., Yates, J. R., 3rd, Oegema, K., Cheeseman, I. M., and Desai, A. (2008) A new mechanism controlling kinetochore-microtubule interactions revealed by comparison of two dynein-targeting components: SPDL-1 and the Rod/Zwilch/Zw10 complex. *Genes Dev.* **22,** 2385–2399 CrossRef Medline
18. Griffis, E. R., Stuurman, N., and Vale, R. D. (2007) Spindly, a novel protein essential for silencing the spindle assembly checkpoint, recruits dynein to the kinetochore. *J. Cell Biol.* **177,** 1005–1015 CrossRef Medline
19. Starr, D. A., Williams, B. C., Hays, T. S., and Goldberg, M. L. (1998) ZW10 helps recruit dynactin and dynein to the kinetochore. *J. Cell Biol.* **142,** 763–774 CrossRef Medline
20. Yamamoto, T. G., Watanabe, S., Essex, A., and Kitagawa, R. (2008) SPDL-1 functions as a kinetochore receptor for MDF-1 in *Caenorhabditis elegans*. *J. Cell Biol.* **183,** 187–194 CrossRef Medline
21. Yang, Z., Tulu, U. S., Wadsworth, P., and Rieder, C. L. (2007) Kinetochore dynein is required for chromosome motion and congression independent of the spindle checkpoint. *Curr. Biol.* **17,** 973–980 CrossRef Medline
22. Simões, P. A., Celestino, R., Carvalho, A. X., and Gassmann, R. (2018) NudE/L regulates dynein at kinetochores but is dispensable for other dynein functions in the *C. elegans* early embryo. *J. Cell Sci.* **131,** jcs212159 CrossRef Medline

23. Vergnolle, M. A., and Taylor, S. S. (2007) Cenp-F links kinetochores to Ndel1/Nde1/Lis1/dynein microtubule motor complexes. *Curr. Biol.* **17,** 1173–1179 CrossRef Medline
24. Li, Y., Yu, W., Liang, Y., and Zhu, X. (2007) Kinetochore dynein generates a poleward pulling force to facilitate congression and full chromosome alignment. *Cell Res.* **17,** 701–712 CrossRef Medline
25. Sharp, D. J., Rogers, G. C., and Scholey, J. M. (2000) Cytoplasmic dynein is required for poleward chromosome movement during mitosis in *Drosophila* embryos. *Nat. Cell Biol.* **2,** 922–930 CrossRef Medline
26. Vorozhko, V. V., Emanuele, M. J., Kallio, M. J., Stukenberg, P. T., and Gorbsky, G. J. (2008) Multiple mechanisms of chromosome movement in vertebrate cells mediated through the Ndc80 complex and dynein/dynactin. *Chromosoma* **117,** 169–179 CrossRef Medline
27. Cheerambathur, D. K., Gassmann, R., Cook, B., Oegema, K., and Desai, A. (2013) Crosstalk between microtubule attachment complexes ensures accurate chromosome segregation. *Science* **342,** 1239–1242 CrossRef Medline
28. DeLuca, J. G., Gall, W. E., Ciferri, C., Cimini, D., Musacchio, A., and Salmon, E. D. (2006) Kinetochore microtubule dynamics and attachment stability are regulated by Hec1. *Cell* **127,** 969–982 CrossRef Medline
29. Cheeseman, I. M., and Desai, A. (2008) Molecular architecture of the kinetochore-microtubule interface. *Nat. Rev. Mol. Cell Biol.* **9,** 33–46 CrossRef Medline
30. Cheeseman, I. M., Chappie, J. S., Wilson-Kubalek, E. M., and Desai, A. (2006) The conserved KMN network constitutes the core microtubule-binding site of the kinetochore. *Cell* **127,** 983–997 CrossRef Medline
31. Ciferri, C., Pasqualato, S., Screpanti, E., Varetti, G., Santaguida, S., Dos Reis, G., Maiolica, A., Polka, J., De Luca, J. G., De Wulf, P., Salek, M., Rappsilber, J., Moores, C. A., Salmon, E. D., and Musacchio, A. (2008) Implications for kinetochore-microtubule attachment from the structure of an engineered Ndc80 complex. *Cell* **133,** 427–439 CrossRef Medline
32. Guimaraes, G. J., Dong, Y., McEwen, B. F., and Deluca, J. G. (2008) Kinetochore-microtubule attachment relies on the disordered N-terminal tail domain of Hec1. *Curr. Biol.* **18,** 1778–1784 CrossRef Medline
33. Sundin, L. J., Guimaraes, G. J., and Deluca, J. G. (2011) The NDC80 complex proteins Nuf2 and Hec1 make distinct contributions to kinetochore-microtubule attachment in mitosis. *Mol. Biol. Cell* **22,** 759–768 CrossRef Medline
34. Welburn, J. P., Vleugel, M., Liu, D., Yates, J. R., 3rd, Lampson, M. A., Fukagawa, T., and Cheeseman, I. M. (2010) Aurora B phosphorylates spatially distinct targets to differentially regulate the kinetochore-microtubule interface. *Mol. Cell* **38,** 383–392 CrossRef Medline
35. Maiato, H., Gomes, A. M., Sousa, F., and Barisic, M. (2017) Mechanisms of chromosome congression during mitosis. *Biology* **6,** E13 CrossRef Medline
36. Kline-Smith, S. L., Sandall, S., and Desai, A. (2005) Kinetochore-spindle microtubule interactions during mitosis. *Curr. Opin. Cell Biol.* **17,** 35–46 CrossRef Medline
37. Tanaka, T. U., and Desai, A. (2008) Kinetochore-microtubule interactions: the means to the end. *Curr. Opin. Cell Biol.* **20,** 53–63 CrossRef Medline
38. Miller, S. A., Johnson, M. L., and Stukenberg, P. T. (2008) Kinetochore attachments require an interaction between unstructured tails on microtubules and Ndc80(Hec1). *Curr. Biol.* **18,** 1785–1791 CrossRef Medline
39. Umbreit, N. T., Gestaut, D. R., Tien, J. F., Vollmar, B. S., Gonen, T., Asbury, C. L., and Davis, T. N. (2012) The Ndc80 kinetochore complex directly modulates microtubule dynamics. *Proc. Natl. Acad. Sci. U.S.A.* **109,** 16113–16118 CrossRef Medline
40. Alushin, G. M., Ramey, V. H., Pasqualato, S., Ball, D. A., Grigorieff, N., Musacchio, A., and Nogales, E. (2010) The Ndc80 kinetochore complex forms oligomeric arrays along microtubules. *Nature* **467,** 805–810 CrossRef Medline
41. Redwine, W. B., Hernandez-Lopez, R., Zou, S., Huang, J., Reck-Peterson, S. L., and Leschziner, A. E. (2012) Structural basis for microtubule binding and release by dynein. *Science* **337,** 1532–1536 CrossRef Medline
42. McKenney, R. J., Huynh, W., Tanenbaum, M. E., Bhabha, G., and Vale, R. D. (2014) Activation of cytoplasmic dynein motility by dynactin-cargo adapter complexes. *Science* **345,** 337–341 CrossRef Medline
43. Raaijmakers, J. A., Tanenbaum, M. E., and Medema, R. H. (2013) Systematic dissection of dynein regulators in mitosis. *J. Cell Biol.* **201,** 201–215 CrossRef Medline
44. DeLuca, J. G., Dong, Y., Hergert, P., Strauss, J., Hickey, J. M., Salmon, E. D., and McEwen, B. F. (2005) Hec1 and nuf2 are core components of the kinetochore outer plate essential for organizing microtubule attachment sites. *Mol. Biol. Cell* **16,** 519–531CrossRef Medline
45. Martin-Lluesma, S., Stucke, V. M., and Nigg, E. A. (2002) Role of Hec1 in spindle checkpoint signaling and kinetochore recruitment of Mad1/Mad2. *Science* **297,** 2267–2270 CrossRef Medline
46. Rieder, C. L., and Alexander, S. P. (1990) Kinetochores are transported poleward along a single astral microtubule during chromosome attachment to the spindle in newt lung cells. *J. Cell Biol.* **110,** 81–95 CrossRef Medline
47. Barisic, M., and Maiato, H. (2015) Dynein prevents erroneous kinetochore-microtubule attachments in mitosis. *Cell Cycle* **14,** 3356–3361 CrossRef Medline
48. Maiato, H., DeLuca, J., Salmon, E. D., and Earnshaw, W. C. (2004) The dynamic kinetochore-microtubule interface. *J. Cell Sci.* **117,** 5461–5477 CrossRef Medline
49. Maiato, H., Rieder, C. L., and Khodjakov, A. (2004) Kinetochore-driven formation of kinetochore fibers contributes to spindle assembly during animal mitosis. *J. Cell Biol.* **167,** 831–840 CrossRef Medline
50. Walczak, C. E., and Heald, R. (2008) Mechanisms of mitotic spindle assembly and function. *Int. Rev. Cytol.* **265,** 111–158 CrossRef Medline
51. DeLuca, J. G., Moree, B., Hickey, J. M., Kilmartin, J. V., and Salmon, E. D. (2002) hNuf2 inhibition blocks stable kinetochore-microtubule attachment and induces mitotic cell death in HeLa cells. *J. Cell Biol.* **159,** 549–555 CrossRef Medline
52. Barisic, M., Sohm, B., Mikolcevic, P., Wandke, C., Rauch, V., Ringer, T., Hess, M., Bonn, G., and Geley, S. (2010) Spindly/CCDC99 is required for efficient chromosome congression and mitotic checkpoint regulation. *Mol. Biol. Cell* **21,** 1968–1981 CrossRef Medline
53. Schaar, B. T., Chan, G. K., Maddox, P., Salmon, E. D., and Yen, T. J. (1997) CENP-E function at kinetochores is essential for chromosome alignment. *J. Cell Biol.* **139,** 1373–1382 CrossRef Medline
54. Wood, K. W., Sakowicz, R., Goldstein, L. S., and Cleveland, D. W. (1997) CENP-E is a plus end-directed kinetochore motor required for metaphase chromosome alignment. *Cell* **91,** 357–366 CrossRef Medline
55. Bennett, A., Bechi, B., Tighe, A., Thompson, S., Procter, D. J., and Taylor, S. S. (2015) Cenp-E inhibitor GSK923295: novel synthetic route and use as a tool to generate aneuploidy. *Oncotarget* **6,** 20921–20932 CrossRef Medline
56. Gassmann, R., Holland, A. J., Varma, D., Wan, X., Civril, F., Cleveland, D. W., Oegema, K., Salmon, E. D., and Desai, A. (2010) Removal of Spindly from microtubule-attached kinetochores controls spindle checkpoint silencing in human cells. *Genes Dev.* **24,** 957–971 CrossRef Medline
57. Winey, M., and Bloom, K. (2012) Mitotic spindle form and function. *Genetics* **190,** 1197–1224 CrossRef Medline
58. Silió, V., McAinsh, A. D., and Millar, J. B. (2015) KNL1-Bubs and RZZ provide two separable pathways for checkpoint activation at human kinetochores. *Dev. Cell* **35,** 600–613 CrossRef Medline
59. Amin, M. A., Kobayashi, K., and Tanaka, K. (2015) CLIP-170 tethers kinetochores to microtubule plus ends against poleward force by dynein for stable kinetochore-microtubule attachment. *FEBS Lett.* **589,** 2739–2746 CrossRef Medline
60. McKenney, R. J., Huynh, W., Vale, R. D., and Sirajuddin, M. (2016) Tyrosination of α-tubulin controls the initiation of processive dynein-dynactin motility. *EMBO J.* **35,** 1175–1185 CrossRef Medline